Romanian Reports in Physics, Vol. 65, No. 3, P. 841–856, 2013

Dedicated to Professor Valentin I. Vlad's 70th Anniversary

EFFECT OF STRESS ON TRAPPING PHENOMENA IN SILICON: FROM SINGLE CRYSTAL TO NANOSTRUCTURES

M.L. CIUREA

National Institute of Materials Physics, P.O.Box MG-7, RO-077125 Bucharest-Magurele, Romania
Academy of Romanian Scientists, Bucuresti 050094, Romania
E-mail: ciurea@infim.ro

Received July 10, 2013

Abstract. In this article, we present and discuss how the stress influences the trapping phenomena in both the bulk Si and nanostructures based on Si. For this, we use single crystal Si irradiated with 28 MeV iodine ions of fluence $(5 \pm 0.5) \times 10^{11}$ ions/cm^2 and 2D Si based nanostructures of $(nc\text{-}Si/CaF_2)_{50}$ multilayers. The method of thermally stimulated discharge currents without bias was employed to investigate the trapping phenomena and the modeling of the discharge current curves was carried out. In the case of irradiated Si, we have modeled the discharge currents considering six trapping levels and a supplementary stress electric field independent of temperature superposed on the frozen-in electric field produced by the charged traps at low temperature. The stress electric field is due to the stopped iodine ions which are heavier than those of Si host. Six traps are evidenced and their parameters are calculated. In the $(nc\text{-}Si/CaF_2)_{50}$ multilayer structures, we experimentally evidenced traps which produce in the discharge current maxima with two shapes. Three maxima have normal shape and the others five maxima are narrow and sharp looking like spikes. We modeled the discharge current curves taking for the concentration a power temperature dependence law, and for the cross section a Gaussian temperature dependence.

Key words: bulk silicon, silicon-based nanostructures, ion irradiation, radiation damage, thermally stimulated currents, point defects, stress induced traps.

1. INTRODUCTION

Silicon and germanium were widely investigated over many decades, starting with electronic devices and then going on with micro- and optoelectronics. At the present, they and other materials based on them are studied in both volume and nanocrystals/nanoparticles to be used in micro- and nanoelectronic devices, photonics, sensors or in biomedical applications [1–17]. A significant advantage for the fabrication of devices based on Si and/or Ge is the Ge compatibility with the Si technology, *e.g.* fabrication of complementary-MOS devices. An important problem which should be taken into account is the presence of defects which determine the performance and reliability of devices.

The defects can be intentionally produced and used in different devices operating or they can appear during the technological processes, being in the most cases detrimental [18–20]. In the bulk Si based detectors, the defects acting as traps are used for the detection of light or heavy nuclear particles, but in fast response silicon devices [21] the defects are produced, as their presence increases the response (switching) speed of these devices. Otherwise, they have a negative effect on the device reliability and performance.

For defects study, different techniques are employed: deep level transient spectroscopy (DLTS) [18–20, 22–30] with its extension of high resolution Laplace transform [19, 20, 23] or charge-DLTS (Q-DLTS) [31], photoinduced current transient spectroscopy (PICTS) and transient-photoconductance derivates (PCD) [32, 33]. Other methods used are the thermally stimulated capacitance [24, 34], the thermally stimulated current with or without bias [35–39]. These techniques give information about activation energy, *i.e.* the depth of trapping levels into the energy band gap, capture cross-section, concentrations and types of defects acting as traps. Besides these defect characterization techniques, current-voltage and capacitance-voltage complementary measurements are performed [20, 26] on diodes with Schottky contacts.

The charge trapping phenomena are studied in different Si and Ge based materials, from bulk to nanostructures. Si and Ge crystals are used for manufacturing dark matter sensor devices or in high-energy physics experiments [40–42].

Many papers appear in the literature studying the damage induced by radiation environment or by implantation on Si host/target, which lead to the formation of defects acting as traps. The defects produced by the irradiation and/or implantation with neutrons [25, 35, 36], H^+ ions [34], He^{++} ions (α-particles) [24, 34, 43], keV Si ions [22], MeV electrons [21], $^{197}Au^{+26}$ or I swift heavy ions [21, 43], or Bi ions [44] on mostly bulk Si crystal and devices, was studied.

The known radiation-induced defects acting as traps in Si are (Si) vacancy-phosphorus atom center, VP, in n-type Si doped with P, vacancy-oxygen complex, VO, divacancies, V_2, centers formed of pairs of interstitial-substitutional carbon, C_i C_s or interstitial carbon-interstitial oxygen, C_i O_i [19, 45]. The knowledge of the temperature at which a defect anneals, meaning the temperature at which the irreversible thermal dissociation of defects takes place, and its activation energy is very important [45].

In bulk Si grown by floating zone and Czochralski methods, other problems related to defects usually appear. Thus, in Ga-doped Si, the iron contamination creates iron-gallium electrically active defects [28], substitutional cobalt and the CoB pair act as traps [23].

Also, the defects were studied in Si-based nanostructures, such as Si supperlattice structures implanted with MeV Si ions [46] to be used in the fabrication of shallow junctions in MOS devices, or in boron- and phosphorus-

doped Si nanowires [33] with the aim to use them in nanoscale Si-based devices. For the Si nanowires, it was shown that the defect levels have the same parameters as in bulk Si [33]. Defects introduced by the electron beam deposition used for contact deposition in epitaxially grown Si were also investigated in comparison with defects introduced by the irradiation with MeV electrons [19]. These metallization-induced defects can be useful for increasing the switching speed of devices or can be detrimental if they are created in high open circuit voltage solar cells.

Charge trapping phenomena are studied on bulk Ge [20, 47] and Ge based-nanostructured materials [29, 31, 48], as well. For example, in Ge MIS capacitors, the density of defects located at the interface between the Ge channel and gate oxide was evaluated [29] with the aim to minimize their concentration by technological operations. The minimum concentration of defects at this interface is a necessary condition in manufacturing Ge-MISFET devices with high channel mobility. Ge nanocrystals embedded in Al_2O_3 or SiO_2 present different energy levels, as it was shown by DLTS measurements, some of them being due to quantum confinement in small Ge nanocrystals, and others to traps at the Ge nanocrystal/amorphous Ge interface [31]. Also, in Sb-mediated Ge QDs embedded in n-type Si, energy levels of the Ge quantum dots were evidenced [48].

The influence of stress on the charge traps parameters is very seldom reported in literature in both, bulk Si and multiquantum well structures or multilayers, as results from the above.

Therefore, in this work we present and discuss how the stress influences the trapping phenomena in both the bulk Si and nanostructures based on Si. For this, we use single crystal Si irradiated with iodine ions and 2D Si based nanostructures of $(nc\text{-}Si/CaF_2)_{50}$ multilayers.

2. SINGLE CRYSTAL SILICON

The irradiation of single crystal Si wafers with ions much bigger and heavier than the Si target, such as the iodine ions, is to be expected to produce besides defects, a local stress as a consequence of their stopping into the Si wafer. In this section the investigation of the traps produced by irradiation with iodine ions are presented and the effect of stress on trapping phenomena is discussed.

2.1. EXPERIMENTAL

The high resistivity n-type Si (more than 8000 Ωcm) wafers doped with P, having 3 ± 0.5^0 off (100) plane orientation, were irradiated with $^{127}I^{6+}$ ions at the Uppsala tandem accelerator. The I ions had 28 MeV kinetic energy, the fluence of $(5 \pm 0.5) \times 10^{11}$ ions/cm^2 [49, 50]. The wafers were scanned in vertical (with 64 Hz) and horizontal (with 517 Hz) directions, and the beam spot had about 2–3 mm diameter.

The samples used for electrical measurements were square pieces of about 0.8 cm length, which were cut from the irradiated wafers. Al contacts were thermally evaporated in a sandwich configuration, the top one being semitransparent (about 50 nm thickness) and the backside one being much thicker (250 nm). For current measurements we used a setup containing a Janis CCS-450 cryostat, a Lakeshore 331 temperature controller, a Keithley 6517A electrometer and a Newport VIS-NIR Cornerstone 260 1/4m monochromator system as a light source.

The thermally stimulated currents (TSC) method without applying external bias was used to investigate the trapping defects produced in the damaged crystalline network of Si by irradiation with iodine ions. This method is adequate to evidence traps in high resistivity semiconductors and nanostructures, and consequently in both single crystal Si and Si based nanostructures [51–54].

2.2. SIMULATION OF PRODUCING DEFECTS BY IRRADIATION WITH IODINE IONS

We simulated the penetration of $^{127}I^{6+}$ ions of 28 MeV in Si wafer by using the Monte Carlo *Crystal-transport and range of ions in matter code* [55] based on the binary collision approximation. It takes into account the effect produced in the Si network by the ion beam with different orientation in respect to the crystalline plane. We considered the penetration of ion beam along the <100> channeling direction and also disoriented in respect to it, with the angles $\theta = 3^o$ and $\varphi = 0.5^o$.

During the penetration of the ion through the Si lattice, it interacts with both the electrons and Si nuclei, and eventually goes to rest. In both processes the ion loses energy, so that its energy is the sum of the energy ultimately given to the electronic and atomic systems, as ionization and atomic motion. The primary self-recoil, created in the first interaction of the ion with a Si nucleus placed in a site of the lattice has a kinetic energy of a few MeV. It initiates a collision cascade, which ends up when the energy imparted to a Si ion in a collision is equal to the threshold for displacements in the lattice [56]. The process of energy partition between the electronic and atomic systems is treated in the frame of Lindhard's model [57]. This way, along the ion track and in the whole volume of the collision cascade, vacancy-interstitial pairs are created [58].

The dependence of the ionization and nuclear energy loss in Si, along the channeling <100> direction and for the direction of interest ($\theta = 3^o$ and $\varphi = 0.5^o$), as obtained from the simulation, are presented in Fig. 1. It could be observed that the range is considerably higher along the direction <100>, in accordance with the theory [57, 59].

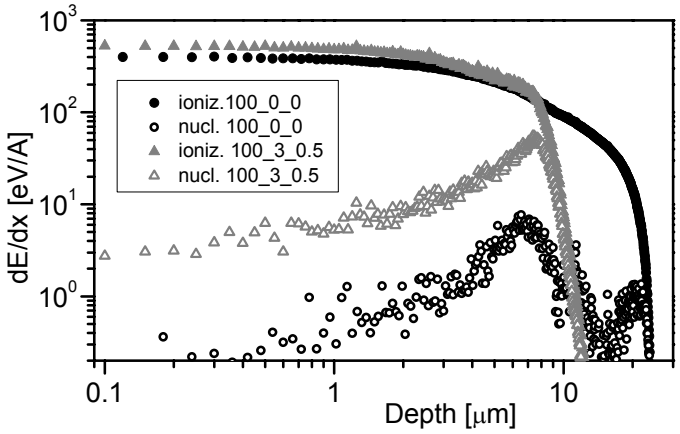

Fig. 1 – Dependence of the ionization and nuclear energy losses by irradiation of Si with I ions considering the <100> channel orientation and the 3 ± 0.5° off orientation [49].

Both vacancies and interstitials created in the cascade have high mobility in silicon, and this is the reason they were not detected at room temperature. The vacancies and interstitials can migrate to sinks or even can annihilate, and finally form 'stable' defects down to depths. The impurities present in our samples are P (~ 5×10^{11} cm^{-3}) from doping, and O and C (both in the range 10^{15} cm^{-3}) from contamination. Consequently, the most probable stable point defects produced by irradiation are V_2, VO, C_iC_s, C_iO_i and VP [60–62]. Their depth distribution, calculated in the frame of a reaction-diffusion model [63, 64], is presented in Fig. 2. As one can see, V_2 and C_iO_i concentrations have a peak at 8 μm depth, the other defects present a concentration plateau down to 10–11 μm. In fact, due to migration of primary defects, *i.e.* vacancies and interstitials, the stable defects will be produced deeper than 10–12 μm in the Si host.

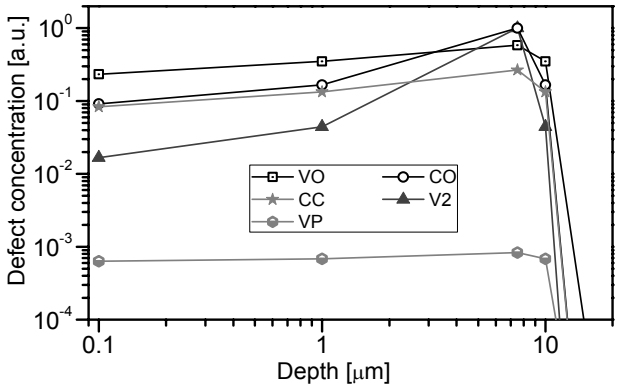

Fig. 2 – Depth distribution of defects resulted from the damage induced by I irradiation on Si host/target [49].

2.3. ELECTRICAL BEHAVIOUR OF DEFECTS PRODUCED BY IRRADIATION WITH IODINE IONS

In general, the experimental investigation of traps using the thermally stimulated currents without externally biasing the samples assume two steps: (1) charging the traps by illuminating the samples at low temperature to hinder the emission of trapped carriers in the energy bands (conduction and/or valence) and (2) controlled discharging the traps by heating the sample with a constant rate up to desired temperature (usually, room temperature, RT). The heating rate should be low enough to ensure the equilibrium of the trap level with the corresponding permitted band. During the heating, the trapped carriers are emitted in energy bands in which they move in the frozen-in electric field produced by the still trapped carriers and so the discharge (thermally stimulated) currents are measured.

In the present case, we charged the traps with monochromatic light of 1000, 800 and 400 nm at 70 K for 20–30 min. The light will be absorbed in the Si samples down to a depth corresponding to the absorption lengths (about 150 μm for 1000 nm, 10 μm for 800 nm and 8 nm for 400 nm) [49, 50]. After switching off the light, the sample was heated up to RT, with a rate of 0.1 K/s, and the discharge current was simultaneously recorded. In the case of Si irradiated with $^{127}I^{6+}$ ions, the electric field in which the detrapped carriers move is the sum between the frozen-in electric field and the field produced by the $^{127}I^{6+}$ ions stopped in the Si host. The iodine ions, being bigger and heavier than those of Si host, produce a local stress and consequently a supplementary electric field induced by stress. The discharge currents curves are presented in Fig. 3. The curve corresponding to 1000 nm illumination (Fig. 3a) presents two main maxima positioned at about 190 and 210 K. The discharge curve after 800 nm illumination (Fig. 3b) is very similar with that obtained for 1000 nm illumination, in contrast with the discharge curve measured after 400 nm illumination (Fig. 3c) in which only the peak positioned at 195 K is evidenced. In the inset in Fig. 3a is shown a small peak around 90 K.

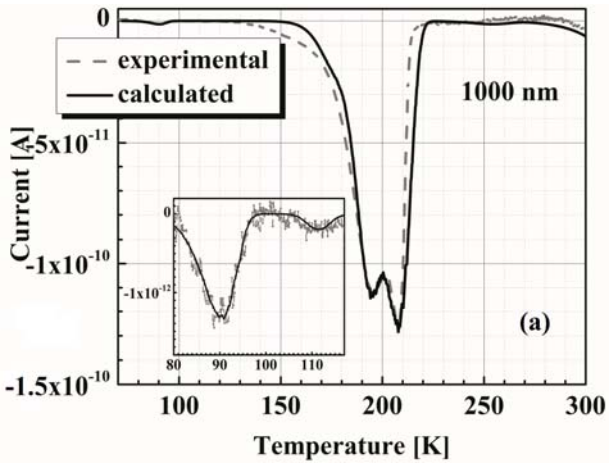

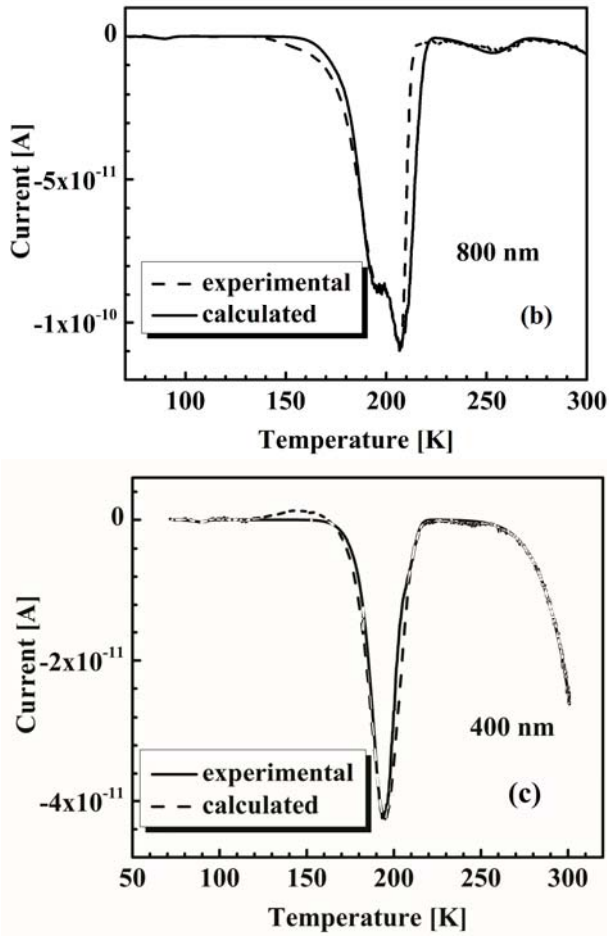

Fig. 3 – Discharge currents curves together with fit ones corresponding to (a) 1000 nm, (b) 800 nm and (c) 400 nm illumination obtained in bulk Si irradiated with $^{127}I^{6+}$ ions [50] (figures reprinted with permission from S. Lazanu, A. Slav, A. M. Lepadatu, I. Stavarache, C. Palade, G. Iordache and M. L. Ciurea, Applied Physics Letters, Vol. 101, Article number 242106 (2012). Copyright 2012, American Institute of Physics).

Fractional heating measurements were performed in order to determine the activation energies of the peaks close to each other. For this, the sample was polarized under the same conditions we used for the integral discharge current curve corresponding for each wavelength. The sample was heated up to 90 K in order to discharge the first maximum (shown in the inset in Fig. 3a). Then, the sample was cooled down at 70 K, and heated again up to the temperature corresponding to the next maximum (195 K) to discharge it, and so on for all maxima. From the slope of the increasing part of the discharge current curves we obtained a set of activation energies of 0.19, 0.28, 0.41–0.45 and 0.51 eV which we

used as start values in the modeling of the integral discharge current curves. These curves were calculated in the frame of the model we previously proposed [52] using MathCAD 14, starting with a system of equations [52, 65] as fallows:

$$\left\{1+\sum_{i'}\tau_{ni'}c_{ni'}(T)\left[N_{ti'}(z,T)-n_{ti'}(z,T)\right]\right\}\frac{\partial}{\partial T}n_{ti}(z,T)=-\frac{1}{\beta}c_{ni}(T)N_{cti}(T)n_{ti}(z,T), \quad (1)$$

$$\Delta n(z,T)\equiv\sum_{i}\Delta n_i(z,T)=\sum_{i}\tau_{ni}c_{ni}(T)N_{cti}(T)n_{ti}(z,T), \quad (2)$$

$$N_{cti}(T)=2\left(\frac{m_e^*k_{\mathrm{B}}T}{2\pi\hbar^2}\right)^{3/2}\exp\left(-\frac{E_c-E_{ti}}{k_{\mathrm{B}}T}\right). \quad (3)$$

In the equations (1) and (2) we used the notations: $n_{ti}(z,T)$ is the concentration of electrons trapped on the level *i*, depending on the depth *z* in the sample (in respect to the illuminated surface) and on the temperature *T* and τ_n is the electron lifetime for which we have taken the same value (100 ns) for all trapping levels. $N_{ti}(z,T)$ is the volume trap concentration, $c_{ni}(T)=\sigma_{ni}(T)\tilde{v}_e(T)$ is the capture coefficient, $\sigma_{ni}(T)$ the capture cross-section and $\tilde{v}_e(T)$ is the mean electron velocity. E_{ti} is the depth of the trapping level into the band gap in respect to the conduction band edge E_c, $\Delta n=n-n_0$ is the volume concentration of detrapped electrons, n_0 - the equilibrium concentration. m_e^* is the effective mass of electrons, k_B and $\hbar$ are Boltzmann and reduced Planck constants, respectively. For holes, similar equations should be considered [52]. In the case of I-irradiated bulk Si we take σ_{ni} independent on temperature.

The electric field under which the carriers move is given by two contributions, one being the frozen-in electric field $E_f(T)$ produced by the charged traps and the second, being the stress electric field E_{iodine} produced by the stopped iodine ions, which we consider independent on temperature [50]:

$$E(T)=E_f(T)+E_{iodine}, \quad (4)$$

$$E_f(T)=ed\frac{\sum_j p_{tj}(T)-\sum_i n_{ti}(T)}{\varepsilon_0\varepsilon_r}, \quad (5)$$

where *e* is the elementary charge, *d* – the depth under the surface with defects, $p_{tj}(T)$ and $n_{ti}(T)$ are the concentrations of holes and electrons, respectively, trapped on the levels *j* and *i* (averaged on *z*), and ε_0 – the vacuum permittivity and ε_r – the relative permittivity of Si.

For the equilibrium carrier concentrations n_0 and p_0 we take the intrinsic concentrations ($n_0 = p_0 = n_i$) as the silicon wafers have high resistivity (more than 8 000 Ω·cm).

In the calculation of the discharge currents, we take into account both detrapped (nonequilibrium) and equilibrium carriers, the last ones having important contribution at high temperatures. The electron current is

$$I_n(T) = -eA[\Delta n(T) + n_i(T)]\mu_n E(T), \tag{6}$$

with A – illuminated area (top electrode area) and μ_n – electron mobility. The hole current has a similar formula depending on hole mobility μ_p.

The thermally stimulated (discharge) currents, obtained for illumination with 1000 and 800 nm, we modeled using a set of six trapping levels. This choice is sustained by the impossibility to resolve some activation energies with a fractionary heating procedure. The curves obtained for 400 nm illumination are modeled with a set of five trapping levels, only, the deepest one (0.53 eV) is no more present in this curve, meaning that the deepest level is located in the sample depth down to the absorption length (8 nm) corresponding to 400 nm illumination. Therefore, at higher temperature, the only existing electric field is that due to the stress, explaining the appearance of the high value current tail in the discharge curves for the 400 nm illumination. By modeling, the cross sections corresponding to all six traps were adjusted at the same time for all the discharge curves corresponding to the three wavelengths. The fit curves together with the experimental curves are presented in Fig. 3. The parameters of all traps are presented in Table 1 in which the trap assignment is according with data reported in the literature.

Table 1

Parameters of the traps obtained from fitting the thermally stimulated (discharge) current curve obtained for 1000 nm illumination [50] with the model described in Ref. [52] (table is reprinted with permission from S. Lazanu, A. Slav, A. M. Lepadatu, I. Stavarache, C. Palade, G. Iordache and M. L. Ciurea, Applied Physics Letters, Vol. 101, Article number 242106, (2012). Copyright 2012, American Institute of Physics)

Trap type	E_t **[eV]**	**Cross section, σ [cm^2]**	**Assigned to**
n	0.17	$1\text{x}10^{-17}$	VO/C_iCs
p	0.30	$1\text{x}10^{-15}$	C_iO_i
n	0.41	$3\text{x}10^{-16}$	V_2
n	0.43	$1\text{x}10^{-16}$	Not assigned
n	0.46	$4.8\text{x}10^{-17}$	VP
n	0.53	$5\text{x}10^{-18}$	Not assigned

The total trap concentration was evaluated for experimental and modeled curves corresponding to the three illumination wavelengths. If the total experimental concentrations were normalized to that obtained for 1000 nm (value normalized to 1), those corresponding to 800 and 400 nm are 0.83 and 0.21, respectively. The concentrations obtained from the theoretical curves are 1/0.91/0.19 for 1000, 800 and 400 nm, in good agreement with the values obtained from experiment.

In conclusion, by irradiation of bulk Si with heavy ions, higher concentrations of trapping defects are produced compared with the irradiation with light particles at similar fluences. This is mainly due to the nuclear energy loss by ions in the Si wafer which produces a bigger damage of the Si host down to the depth they are stopped. We started to investigate the effect of the irradiation of Si with $^{209}Bi^{6+}$ ions with the same fluence as used for irradiation with iodine [66]. The concentration of the defects produced by Bi irradiation is higher in comparison with the defect concentration produced by I irradiation, and the stress field produced by Bi ions stopped in Si structure is higher, too. This is sustained by the penetration depth of Bi, smaller than that of I.

3. SILICON-BASED NANOSTRUCTURES

In the case of nanostructures, the stress generally appears in multilayers at the interfaces between layers of different materials due to the different expansion coefficients. In this section we present the effect of stress in 2D $(nc\text{-}Si/CaF_2)_{50}$ multilayer structures which induces traps of whose effect is the appearance of very sharp peaks/spikes in the discharge current curves.

3.1. EXPERIMENTAL

The multilayer 2D structures formed of 50 pairs of nc-Si/CaF_2 layers were deposited on n-type (111) Si by molecular beam epitaxy [67]. Both nc-Si and CaF_2 layers in the pair are formed of nanocrystals. Each nc-Si layer has the same thickness as CaF_2 one (g = 1.6 nm). For electrical measurements, a transparent Al top electrode and a thick bottom one were thermally deposited.

The thermally stimulated current method without bias was used for the investigation of trapping phenomena as in the case of Si wafers irradiated with iodine ions. The samples were illuminated with 500 nm wavelengths at liquid nitrogen temperature, and the discharge currents were measured by heating the sample with a rate of 0.1 K/s.

3.2. STRESS-INDUCED TRAPS IN $(nc\text{-}Si/CaF_2)_{50}$ MULTILAYER STRUCTURES

In these structures we evidenced two kinds of maxima in the thermally stimulated discharge current curves. The maxima of the one type have a normal shape and they are produced by the discharge of the “normal” traps, and the other maxima look like spikes (narrow and sharp) and are produced by the stress-induced traps as it will be demonstrated hereafter. Because the spikes are produced by the different expansion coefficients of the nc-Si and CaF_2 layers, the corresponding traps should be located at the interface between these layers.

The photogenerated carriers diffuse into the nc-Si layers and fully fill the traps (CaF_2 is transparent to 500 nm wavelength) at low temperature. In Fig. 4 the experimental curve obtained for 500 nm illumination is shown. The curve was filtered using the procedure of optimal linear smoothing (POLS), described in Ref. [68] and applied in Ref. [65]. In this figure one can see three normal peaks and five spikes.

We modeled the discharge current curves using the system of equations (1−3) and hypothesis that the concentration of the traps and trapped carriers is independent on the depth z into the multilayer structure. This hypothesis is sustained by the homogeneity of the layers in respect to z and the complete filling of the traps by the illumination. The normal maxima were described in the same terms as in the bulk Si, but for the spikes we considered that the concentration of the trapping centers and cross sections are temperature dependent fallowing a power law for $N_{ti}(T)$ and a Gaussian form for σ_{ni} [65, 69]:

$$N_{ti}(T) = N_{ti}^{(0)}\left(1-\frac{T}{T_s}\right)^{\gamma_{ni}}, \tag{7}$$

$$\sigma_{ni} = \sigma_{ni}^{(0)}\exp\left(-\frac{(T-T_{ni})^2}{2W_{ni}^2}\right), \tag{8}$$

Similar equations can be written for holes. In Eqs. 7 and 8, T_s is the storage temperature. The exponents γ_{ni} for electrons (as well as for holes) and the half-widths W_{ni} (and W_{pj}, too) are considered to be independent on the trap charge sign and take the values $\gamma_{ni} = \gamma_{pj} = 4$ and $W_{ni} = W_{pj} = \sqrt{2}$ K. The trap concentration for electrons, $N_{ti}(T)$ is a volume concentration, so that by multiplying it with the (nc-Si or CaF_2) film thickness g, the surface concentration of the traps located at the interface is obtained. The cross section for the stress-induced traps is plausible to be of a Gaussian form in the frame of the thermodynamical fluctuation theory.

The frozen-in electric field is:

$$\widetilde{E}(T) = \frac{2q+1}{4}\frac{eg}{\varepsilon_0\varepsilon_r}\left[p_t(T)-n_t(T)\right], \tag{9}$$

where q = 50 (number of paired layers), ε_r is the relative permittivity of CaF_2, $p_t(T)=\sum_j p_{tj}(T)$ and $n_t(T)=\sum_i n_{ti}(T)$.

From the five current contributions (the conduction/ohmic current given by the equilibrium carriers n_0, current given by the non-equilibrium carriers due to the detrapping, diffusion current, tunneling current and displacement current), through this multilayer structure [52, 70], only tunneling (I_t) and displacement (I_d)

currents flow because the CaF_2 layers are insulators and the structure is homogeneous (the diffusion current is null), so that the total current is $I = I_t + I_d$:

$$I_t = \text{sign}\left(\tilde{U}\right)\left\{ I_n \left[\left(1 - \frac{\left|\tilde{U}\right|}{U_n} \right) \exp\left(-\alpha_n \sqrt{1 - \frac{\left|\tilde{U}\right|}{U_n}} \right) - \exp\left(-\alpha_n\right) \right] - \right.$$
$$\left. - I_p \left[\left(1 + \frac{\left|\tilde{U}\right|}{U_p} \right) \exp\left(-\alpha_p \sqrt{1 + \frac{\left|\tilde{U}\right|}{U_p}} \right) - \exp\left(-\alpha_p\right) \right] \right\}, \tag{10}$$

$$I_d = \varepsilon_0 \varepsilon_r A \beta \frac{d\tilde{E}}{dT}, \tag{11}$$

in which $\tilde{U}(T) = 2g\tilde{E}(T)$ is the mean bias per CaF_2 layer, $I_n = enA\tilde{v}_e/\sqrt{3}$, $I_p = epA\tilde{v}_h/\sqrt{3}$, $\alpha_n = \sqrt{8em_e^* U_n g^2/\hbar^2}$, $\alpha_p = \sqrt{8em_h^* U_p g^2/\hbar^2}$, and eU_n and eU_p represent the barrier heights tunneled by electrons and holes [65].

In Fig. 4 is also given the theoretical curve obtained for the 500 nm illumination, taking for the carrier lifetimes the values $\tau_n = 400$ ns and $\tau_p = 180$ ns. The trap parameters obtained from modeling are given in the Table 2.

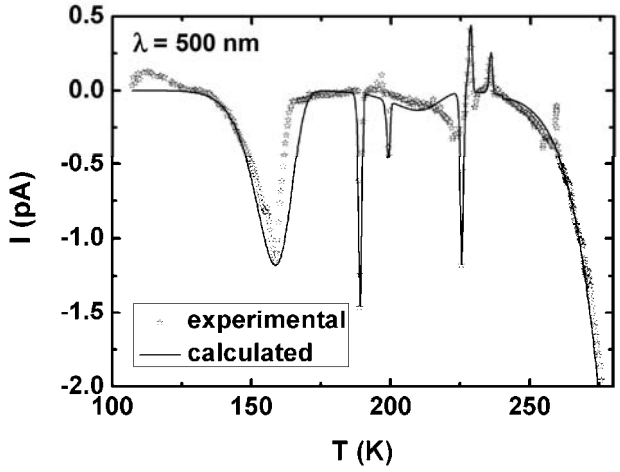

Fig. 4 – Discharge currents curves together with fit corresponding to 500 nm illumination obtained in $(nc\text{-}Si/CaF_2)_{50}$ multilayer structures [65] (figure reprinted with permission from M. L. Ciurea, S. Lazanu, I. Stavarache, A.-M. Lepadatu, V. Iancu, M. R. Mitroi, R. R. Nigmatullin and M. C. Baleanu, Journal of Applied Physics, Vol. 109, Article number 013717, (2011). Copyright 2011, American Institute of Physics).

Table 2

Parameters of the traps obtained from fitting with the model the thermally stimulated (discharge) current curve obtained for 500 nm illumination [65]

Trap type	E_t **(eV)**	$\sigma^{(0)}$ **(10^{-18} cm^2)**	T_n, T_p **(K)**	$N_t^{(0)}, P_t^{(0)}$ **(10^{15} cm^{-3})**
n	0.30	1.3	–	0.375
n	0.36	50	192	3.2
n	0.38	50	202	1.3
n	0.41	1.0	–	0.08
n	0.42	50	229	12.5
p	0.44	50	232	4.1
p	0.45	50	239	3.5
n	0.63	1.6	–	75

We have to remark that by filtering the curves using the POLS procedure, all maxima and spikes given by the discharge of the traps are put in evidence, otherwise some spikes appear as noise features.

4. CONCLUSIONS

In this paper we studied the influence of stress on the trapping phenomena in bulk Si and 2D Si based nanostructures of (nc-Si/CaF_2)$_{50}$ multilayers by using the method of thermally currents without bias and by modeling the discharge currents.

For this, we investigated the stress produced by the Si irradiation with $^{127}I^{6+}$ ions which are bigger and heavier than Si atoms, and the stress which appears in the multilayers structures at the nc-Si/CaF_2 interfaces due to the different expansion coefficients of any adjacent layers.

In the bulk Si irradiated with $^{127}I^{6+}$ ions the concentration of the defects/traps is bigger than that in Si irradiated with light particles. This is because, the I ions produce a stronger damage of Si network and consequently a bigger concentration of defects. The I ions stopped in the Si target produce a local deformation leading to the appearance of a permanent electric field, independent on temperature. This stress field tunes the discharge current by its superposition on the frozen-in electric field produced by the charged traps at low temperature.

In the (nc-Si/CaF_2)$_{50}$ multilayer structures, the stress produced by the different expansion coefficients of the adjacent nc-Si and CaF_2 layers induces new traps, located at the nc-Si/CaF_2 interface. The discharge currents due to the stress induced traps present maxima with typical shape of spikes (narrow and sharp). The parameters of stress induced traps are dependent on temperature, so that the concentration fallows a power law, and the cross section has a Gaussian dependence.

Acknowledgements. This work was supported by the Romanian Ministry of National Education through the CNCS – UEFISCDI under contract no. PCCE-ID-76 and through the NIMP Core Programme PN09-450101.

REFERENCES

1. S. K. Ray, S. Maikap, W. Banerjee and S. Das, J. Phys. D: Appl. Phys., **46**, 153001 (2013).
2. P. Liu, S. Cosentino, S. T. Le, S. Lee, D. Paine, A. Zaslavsky, D. Pacifici, S. Mirabella, M. Miritello, I. Crupi and A. Terrasi, J. Appl. Phys., **112**, 083103 (2012).
3. M. T. Trinh, R. Limpens, W. D. A. M. de Boer, J. M. Schins, L. D. A. Siebbeles and T. Gregorkiewicz, Nat. Photonics, **6**, 316 – 321 (2012).
4. I. Stavarache, A.-M. Lepadatu, A. V. Maraloiu, V. S. Teodorescu and M. L. Ciurea, J. Nanopart. Res., **14**, 930 (2012).
5. D. Di, I. Perez-Wurfl, L. Wu, Y. Huang, A. Marconi, A. Tengattini, A. Anopchenko, L. Pavesi and G. Conibeer, Appl. Phys. Lett., **99**, 251113 (2011).
6. R. Pillarisetty, Nature, **479**, 324–328 (2011).
7. I. Stavarache, A.-M. Lepadatu, N. G. Gheorghe, R. M. Costescu, G. E. Stan, D. Marcov, A. Slav, G. Iordache, T. F. Stoica, V. Iancu, V. S. Teodorescu, C. M. Teodorescu and M. L. Ciurea, J. Nanopart. Res., **13**, 221–232 (2011).
8. Z. C. Holman, C. Y. Liu and U. R. Kortshagen, Nano Lett., **10**, 2661–2666 (2010).
9. G. Katsaros, P. Spathis, M. Stoffel, F. Fournel, M. Mongillo, V. Bouchiat, F. Lefloch, A. Rastelli, O. G. Schmidt and S. De Franceschi, Nat. Nanotechnol., **5**, 458–464 (2010).
10. V. S. Teodorescu, M. L. Ciurea, V. Iancu and M.-G. Blanchin, J. Mater. Res. **23**, 2990–2995 (2008).
11. C. Popa, R. Turcu, I. Craciunescu, A. Nan, M. L. Ciurea, I. Stavarache and V. Iancu, J. Optoelectron. Adv. Mater., **10**, 2319–2324 (2008).
12. G. Conibeer, M. Green, R. Corkish, Y. Cho, E. C. Cho, C. W. Jiang, T. Fangsuwannarak, E. Pink, Y. Huang, T. Puzzer, T. Trupke, B. Richards, A. Shalav and K. Lin, Thin Solid Films, **511-512**, 654–662 (2006).
13. M. L. Ciurea, V. S. Teodorescu, V. Iancu and I. Balberg, Chem. Phys. Lett., **423**, 225–228 (2006).
14. V. Iancu, M. Draghici, L. Jdira and M. L. Ciurea, J. Optoelectron. Adv. Mater., **6**, 53–56 (2004).
15. M. L. Ciurea, M. Draghici, V. Iancu, M. Reshotko and I. Balberg, J. Luminesc., **102-103**, 492–497 (2003).
16. M. L. Ciurea, V. Iancu, V. Teodorescu, L. Nistor and M. G. Blanchin, J. Electrochem. Soc., **146**, 3516–3521 (1999).
17. M. L. Ciurea, I. Baltog, M. Lazar, V. Iancu, S. Lazanu and E. Pentia, Thin Solid Films, **325**, 271–277 (1998).
18. T. Mchedlidze, M. Kittler, J. Appl. Phys., **111**, 053706 (2012).
19. F. D. Auret, S. M. M. Coelho, J. M. Nel and W. E. Meyer, Phys. Status Solidi, **A 209**, 1926–1933 (2012).
20. C. Nyamhere, A. G. M. Das, F. D. Auret, A. Chawanda, W. Mtangi, Q. Odendaal and A. Carr, Physica, **B 404**, 4379–4381 (2009).
21. N. A. Poklonski, N. I. Gorbachuk, S. V. Shpakovski, A. V. Petrov, S. B. Lastovskii, D. Fink and A. Wieck, Nucl. Instr. Meth. Phys. Res., **B 266**, 5007–5012 (2008).
22. C. Nyamhere, F. Cristiano, F. Olivie, Z. Essa, E. Bedel-Pereira, D. Bolze and Y. Yamamoto, J. Appl. Phys., **113**, 184508 (2013).
23. L. Scheffler, Vl. Kolkovsky and J. Weber, J. Appl. Phys., **113**, 183714 (2013).
24. Kh. A. Abdullin, B. N. Mukashev, Physica, **B 407**, 2508–2511 (2012).
25. A. Junkes, I. Pintilie, E. Fretwurst and D. Eckstein, Physica, B **407**, 3013–3015 (2012).
26. D. W. Kwak, D. W. Lee, J. S. Oh, Y. H. Lee and H. Y. Cho, Thin Solid Films, **520**, 5593–5596 (2012).

27. E. Simoen, V. Depauw, I. Gordon and J. Poortmans, Phys. Status Solidi, **A 209**, 1857–1860 (2012).
28. Y. Yoon, Y. Yan, N. P. Ostrom, J. Kim and G. Rozgonyi, Appl. Phys. Lett., **101**, 222107 (2012).
29. D. Wang, S. Kojima, K. Sakamoto, K. Yamamoto and H. Nakashima, J. Appl. Phys., **112**, 083707 (2012).
30. A. V. P. Coelho, M. C. Adam and H. Boudinov, J. Phys. D: Appl. Phys., **44**, 305303 (2011).
31. I. V. Antonova, V. I. Popov, S. A. Smagulova, J. Jedrzejewski and I. Balberg, J. Appl. Phys,. **113**, 084308 (2013).
32. Y. Hu, H. Schøn, Ø. Nielsen, E. J. Øvrelid and L. Arnberg, J. Appl. Phys., **111**, 053101 (2012).
33. K. Sato, A. Castaldini, N. Fukata and A. Cavallini, Nano Lett., **12**, 3012 − 3017 (2012).
34. Yu. V. Gorelkinskii, Kh. A. Abdullin, B. N. Mukashev and T. S. Turmagambetov, Physica, B **404**, 4579–4582 (2009).
35. V. Sopko, B. Sopko, J. Dammer and D. Chren, J. Inst., **6**, C12020 (2011).
36. D. Menichelli, R. Mori, M. Scaringella and M. Bruzzi, Nucl. Instr. Meth. Phys. Res., **A 612**, 530–533(2010).
37. D. Petre, I. Pintilie, M. L. Ciurea and T. Botila, Thin Solid Films, **260**, 54–57 (1995).
38. D. Petre, I. Pintilie, M. L. Ciurea and T. Botila, J. Appl. Phys., **76**, 2216–2219 (1994).
39. D. Valentovic, J. Cervenak, S. Luby, M. L. Aldea and T. Botila, Phys. Stat. Sol., **(a) 56**, 341–347 (1979).
40. I. Lazanu, M. L. Ciurea and S. Lazanu, Astropart. Phys., **44**, 9–14 (2013).
41. S. Lazanu, M. L. Ciurea and I. Lazanu, Phys. Status Solidi (c), **6**, 1974–1978 (2009).
42. E. Previtali, Nucl. Phys. B (Proc. Suppl.), **150**, 3–8 (2006).
43. L. Vines, E. V. Monakhov, J. Jensen, A. Yu. Kuznetsov and B. G. Svensson, Phys. Rev. B, **79**, 075206 (2009).
44. C. D. Weis, C. C. Lo, V. Lang, A. M. Tyryshkin, R. E. George, K. M. Yu, J. Bokor, S. A. Lyon, J. J. L. Morton and T. Schenkel, Appl. Phys. Lett., **100**, 172104 (2012).
45. G. P. Gaidar, Surf. Eng. Appl. Electrochem. **48**, 78–89 (2012).
46. L. Shao, P. E. Thompson, Q. Y. Chen, K. B. Ma, J. R. Liu and W.-K. Chu, Appl. Phys. Lett., **93**, 041908 (2008).
47. C. Nyamhere, A. Venter, D. M. Murape, F. D. Auret, S. M. M. Coelho and J. R. Botha, Physica B, **407**, 2935–2938 (2012).
48. V.-T. Rangel-Kuoppa, A. Tonkikh, P. Werner and W. J. Rangel-Kuoppa, Appl. Phys. Lett., **102**, 232106 (2013).
49. A. Slav, A.-M. Lepadatu, C. Palade, I. Stavarache1, G. Iordache, M. L. Ciurea, S. Lazanu and M. R. Mitroi, *Semiconductor Conference* (CAS), 2012 International, **2**, 273–276 (2012).
50. S. Lazanu, A. Slav, A. M. Lepadatu, I. Stavarache, C. Palade, G. Iordache and M. L. Ciurea, Appl. Phys. Lett., **101**, 242106 (2012). (Figures 2, 3 and 4, Equations 3, 4 and 5 and Table 2 are reproduced and reprinted with permission from S. Lazanu, A. Slav, A. M. Lepadatu, I. Stavarache, C. Palade, G. Iordache and M. L. Ciurea, Applied Physics Letters, Vol. 101, Article number 242106, (2012). Copyright 2012, American Institute of Physics).
51. M. L. Ciurea, Proc. Romanian Acad. A, **12**, 315–323 (2011).
52. M. L. Ciurea, V. Iancu and M. R. Mitroi, Solid–State Electron., **51**, 1328–1337 (2007). (Equations 1 and 2 are reproduced from Solid–State Electron. Vol 51, M. L. Ciurea, V. Iancu and M. R. Mitroi, Trapping phenomena in silicon-based nanocrystalline semiconductors, pp. 1328–1337, Copyright 2007, with permission from Elsevier).
53. M. Draghici, M. Miu, V. Iancu, A. Nassiopoulou, I. Kleps, A. Angelescu and M. L. Ciurea, Phys. Stat. Sol., **(a) 182**, 239–243 (2000).
54. M. L. Ciurea, M. Draghici, S. Lazanu, V. Iancu, A. Nasiopoulou, V. Ioannou and V. Tsakiri, Appl. Phys. Lett. **76**, 3067–3069 (2000).
55. Crystal-TRIM (04/1D-last revision May 2004), developed by Matthias Posselt, Forschungszentrum Rossendorf, Dresden, Germany, 1991-2005.
56. S. Lazanu, I. Lazanu, Nucl. Instr. Meth. Phys. Res., **A 462**, 530–535 (2001).

57. J. Lindhard, V. Nielsen, M. Schraff and P.V. Thomsen, *Integral equations governing radiation effects*, Mat. Fys. Medd. Dan. Vid. Selsk, **33**, 1–42 (1963).
58. S. Lazanu, I. Lazanu, J. Optoel. Adv. Mat., **9**, 1839–1842 (2007).
59. M. A. Kumakhov, Radiat. Eff., **26**, 43–48 (1975).
60. M. L. Ciurea, V. Iancu, S. Lazanu, A.-M. Lepadatu, E. Rusnac and I. Stavarache, Rom. Rep. Phys., **60**, 735–748 (2008).
61. I. Lazanu, S. Lazanu, Nucl. Instr. Meth. Phys. Res., **B 201**, 491–502 (2003).
62. I. Lazanu, S. Lazanu, Physica Scripta, **66**, 125–132 (2002).
63. S. Lazanu, I. Lazanu, Nucl. Instr. Meth. Phys Res., **A 583**, 165–168 (2007).
64. I. Lazanu, S. Lazanu, Phys. Scripta, **74**, 201–207 (2006).
65. M. L. Ciurea, S. Lazanu, I. Stavarache, A.-M. Lepadatu, V. Iancu, M. R. Mitroi, R. R. Nigmatullin and M. C. Baleanu, J. Appl. Phys., **109**, 013717 (2011). (Equations 9 and 10 and Fig. 4 are reproduced and reprinted with permission from M. L. Ciurea, S. Lazanu, I. Stavarache, A.-M. Lepadatu, V. Iancu, M. R. Mitroi, R. R. Nigmatullin and M. C. Baleanu, Journal of Applied Physics, Vol. 109, Article number 013717, 2011. Copyright 2011, American Institute of Physics.
66. C. Palade, A. Slav, M. L. Ciurea and S. Lazanu, *Semiconductor Conference* (CAS), 2013 International, accepted.
67. V. Ioannou-Sougleridis, A. G. Nassiopoulou, M. L. Ciurea, F. Bassani and F. A. d'Avitaya, Mater. Sci. Eng., **C 15**, 45–47 (2001).
68. R. R. Nigmatullin, *New Noninvasive Methods for 'Reading' of Random Sequences and Their Applications in Nanotechnology*, editors D. Baleanu, Z. B. Guvenc, J. A. T. Machado, in *New trends in nanotechnology and fractional calculus applications*, Springer-Verlag Berlin, 2010, pp. 43–56.
69. A.-M. Lepadatu, I. Stavarache, S. Lazanu, V. Iancu, M. R. Mitroi, R. R. Nigmatulin and M. L. Ciurea, *Semiconductor Conference* (CAS), 2010 International, **2**, 371–374 (2010).
70. V. Iancu, M. L. Ciurea and M. Draghici, J. Appl. Phys., **94**, 216–223 (2003).